A Model for Imbibition in Pore Spaces from 2D Rock Images

Yingfang Zhou[1*], Johan O. Helland[2], Dimitrios G. Hatzignatiou[3]

1 International Research Institute of Stavanger (IRIS) & University of Stavanger (UIS), *e-mail: yizh@iris.no*
2 International Research Institute of Stavanger (IRIS), *e-mail: joh@iris.no*
3 International Research Institute of Stavanger (IRIS) & University of Stavanger (UIS), *e-mail: dh@iris.no*
** Corresponding author*

Abstract — A Model for Imbibition in Pore Spaces from 2D Rock Images— *We model viscous- and capillary-controlled fluid displacement directly in 2D rock images by considering the identified pore spaces as cross-sections in a bundle of capillary tubes. The phase pressures vary with length positions but remain unique in each cross-section; this leads to a nonlinear system of equations that are solved for the interface positions as a function of time. The cross-sectional fluid configurations are computed accurately at any capillary pressure and wetting condition by a semi-analytical model. Evolution of saturation profiles during imbibition is simulated for different wetting conditions, viscosity ratios and injection rates. An attractive feature of the model is the opportunity to evaluate the effects of pore-scale mechanisms on macro-scale properties because the flow simulations and required input data are calculated consistently in identical geometries.*

INTRODUCTION

Waterflood oil recovery and transient behaviour in reservoir cores are normally analysed with one-dimensional core-scale models. In such models, phase-pressure equilibration exists in both the water and oil phases along the distance from the inlet boundary. This feature is captured in the interacting tube bundle model proposed by Dong *et al.* [1] and Wang and Dong [2], where the phase pressures vary with length positions but remain unique in each cross-section. This model represents the core section by idealised pore shapes, and hence appropriate pore-size distributions are required as input to make quantitative comparisons with realistic experiments. The assumption of phase pressure uniqueness in each cross-section causes the meniscus with largest capillary pressure and velocity to advance in front [1]. This is in agreement with core-scale models that are based on the standard multiphase extension of Darcy's law [5].

In this work, an interacting tube bundle model for water flooding is developed, in which the pore space geometry in the core section is represented by 2D rock images. This is accomplished by extending a semi-analytical model for entry pressure calculations [3] to account for simulations of complete capillary pressure curves, and by computing the conductance in the corresponding fluid configurations. The interacting tube bundle algorithm is modified accordingly to allow the capillary pressure, fluid configuration and conductance data to be given as input. Evolution of saturation profiles are simulated at different conditions and the results are related to the pore-scale displacement mechanisms occurring in the 2D rock images.

1 INTERACTING TUBE BUNDLE MODEL

In the interacting tube bundle model, the resolution of the saturation front, i.e., front menisci, and capillary pressure data is equal. For $k = 1, \ldots, N$ front menisci with capillary pressures $p_{c,k}$, the tube bundle is divided into $N+1$ length regions, where in each region k the cross-sectional fluid areas, $A_{o,k}$ and $A_{w,k}$, and fluid conductances, $g_{o,k}$ and $g_{w,k}$, are constant. Figure 1 shows a schematic of the front menisci positions x_k measured from the reservoir inlet. In the same figure, a realistic cross-sectional fluid configuration in a length region is shown to the right, as computed by the semi-analytical model. A sketch of the phase pressure profiles along the tube bundle is also illustrated in Figure 2. Hence, the pressure difference Δp between the water (reservoir inlet) and oil (reservoir outlet) can be expressed in terms of the capillary pressure across each front meniscus and the phase pressure differences in each region. This yields N pressure equations:

$$\sum_{i=1}^{k} \Delta p_{w,i} + \sum_{i=k+1}^{N+1} \Delta p_{o,i} = p_{c,k} + \Delta p. \qquad (1)$$

The flow rates of oil and water, $q_{o,k}$ and $q_{w,k}$, are expressed in the $N+1$ regions by a general Hagen-Poiseuille equation,

$$q_{o,k} = g_{o,k} \frac{\Delta p_{o,k}}{x_k - x_{k-1}}, \; q_{w,k} = g_{w,k} \frac{\Delta p_{w,k}}{x_k - x_{k-1}}, \qquad (2)$$

and by material balance as

$$q_{o,k} = \sum_{i=1}^{k-1} \Delta A_{o,i} \frac{\Delta x_i}{\Delta t}, \; q_{w,k} = \sum_{i=k}^{N} \Delta A_{o,i} \frac{\Delta x_i}{\Delta t}. \qquad (3)$$

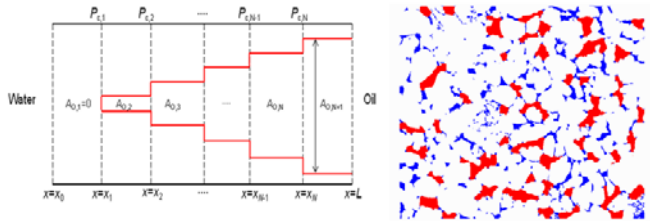

Figure 1: Schematic of the interface positions along the tube bundle (left), and cross-sectional fluid configuration in a length region as computed by the semi-analytical model (right).

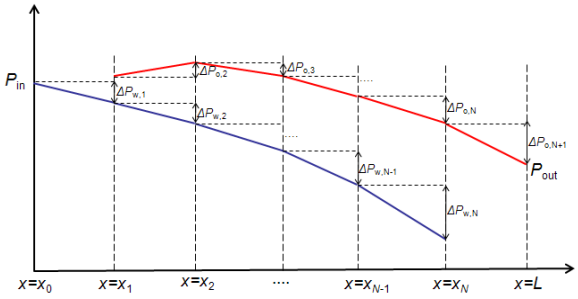

Figure 2: Oil- and water-phase pressure profiles along the tube bundle.

The water flow rate could also be expressed in terms of injection rate as follows:

$$q_{w,1} = q_{tot}, \ldots, q_{w,k} = q_{tot} - q_{o,k}, \ldots, q_{w,N+1} = 0 \qquad (4)$$

Eqs. (2) and (3) are combined and inserted into Eq. (1) yielding a system of N nonlinear equations that is solved for the N unknown interface positions x_k when Δp is constant. For constant rate displacements, the injection rate q_{tot} is given as an input parameter, whereas Δp varies with displacement time. In this case, the constant injection rate condition

$$q_{tot} = q_{w,1} = \sum_{i=1}^{N} \Delta A_{o,i} \frac{\Delta x_i}{\Delta t} \qquad (5)$$

provides an additional equation, and a system of $N+1$ equations is solved at various time steps by Newton-Raphson iterations for the $N+1$ unknown parameters $x_k, k = 1, \ldots, N$ and Δp.

Simulations with the interacting tube bundle model require $p_{c,k}$, $A_{o,k}$, $g_{o,k}$ and $g_{w,k}$, $k = 1, \ldots, N$ as input data. The capillary pressures and fluid configurations are computed by the semi-analytical model which is based on extending the MS-P method [4] to allow for arbitrary pore shapes from 2D rock images as tube cross-sections.

2 SEMI-ANALYTICAL PORE-SCALE MODEL

The procedure begins by computing smooth pore-boundary points b and associated orientation angles $\alpha(b)$ in the rock image. Then, for each given capillary pressure $p_c = \sigma / r$, a circle with radius r is moved along the pore boundary in opposite directions with the contact angle θ defined at the front arcs. The loci of circle centres constitute two closed curves given by:

$$v^{cc} = (x - r\sin(\alpha+\theta), y + r\cos(\alpha+\theta)),$$
$$v^{c} = (x - r\sin(\alpha-\theta), y + r\cos(\alpha-\theta)). \qquad (6)$$

Intersections of these curves determine the geometrically allowed arc menisci (AM) and their corresponding contact lines at the given capillary pressure. Geometrical regions, with boundaries composed of alternate pore-wall segments and AM, are determined by a pore-boundary tracking procedure. These regions are classified as bulk phase regions (BR) or layer phase regions (LR) based on the orientation of the AM that belong to the region boundaries.

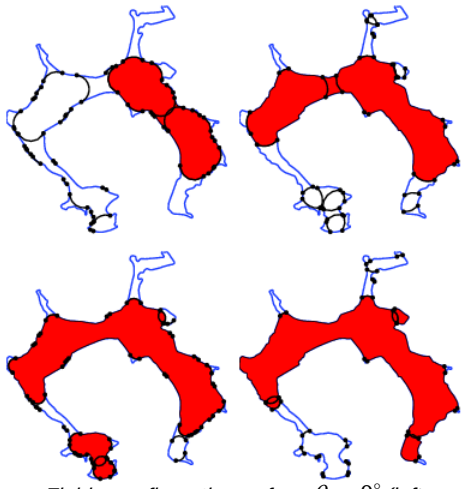

Figure 3: Fluid configurations for $\theta = 0^\circ$ (left column) and $\theta = 40^\circ$ (right column) in a pore space extracted from Bentheim sandstone. Regions coloured red are invaded by oil, and the uncoloured parts remain water filled. The fluid configurations are compared at entry pressure (top row) and at higher pressures (bottom row), and the effects of wettability is clearly visible.

The valid fluid configuration change is associated with the most favourable entry pressure among all possible displacement scenarios. Therefore, entry pressures are computed for all valid BR and LR combinations that have not become occupied by the invading fluid yet. The general MS-P equation for region combination i is given by

$$F_i(r) = \frac{L_{os,i}\cos\theta + L^E_{ow,i} - L^F_{ow,i}}{A_{inv,i}}, \qquad (7)$$

where $L^E_{ow,i}$ and $L^F_{ow,i}$ are the lengths of the AM that form and vanish during the displacement, respectively. The solid length contacted by the invading fluid is given by $L_{os,i}$, and $A_{inv,i}$ is the invaded cross-sectional area.

The fluid configuration at a given capillary pressure is determined by an iterative procedure where, in each

iteration step, the most favourable entry pressure among all available displacement scenarios N_c is determined by

$$F^*(r) = \min\left\{F_i(r) : 1/r \geq F_i(r), i = 1, \ldots, N_c\right\}, \qquad (8)$$

and the corresponding region combination is invaded by oil. The iterations are terminated when $F^*(r)$ cannot be determined, and the algorithm proceeds with the next capillary pressure. An example of computed fluid configurations in an irregular pore space is presented in Figure 3 for different wetting conditions. The total cross-sectional oil areas obtained at specified capillary pressures are given as input to the interacting tube bundle model.

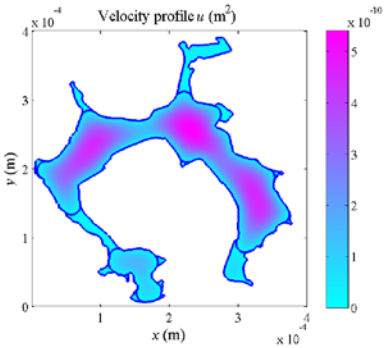

Figure 4: Oil and water velocity profiles calculated by applying Matlab PDE Toolbox directly in the extracted Bentheim sandstone pore space. The fluid configuration is determined by the semi-analytical model.

3 CONDUCTANCE COMPUTATION

Pore space-, oil- and water conductances are obtained by computing the velocity profile directly in each cross-sectional fluid configuration determined by the semi-analytical model. Steady-state, laminar flow of incompressible fluids with constant viscosity and no-slip conditions at all boundaries are assumed. These computations are performed by applying MATLAB Partial Differential Equation Toolbox on many different pore space geometries and fluid configurations. A numerical example is shown in Figure 4. Based on the obtained data, physically-sound conductance correlations are formulated as functions of areas A and shape factors :

$$\frac{g_p}{A_p^2} = -3.1668G_p^2 + 0.7485G_p, \quad \text{(pore space)}$$

$$\frac{g_o}{g_p} = -0.8\left(\frac{A_o}{A_p}\right)^3 + 0.6\left(\frac{A_o}{A_p}\right)^2 + 1.2\left(\frac{A_o}{A_p}\right), \quad \text{(oil)} \qquad (9)$$

$$\frac{g_w}{A_w^2} = -4.008G_w^2 + 0.7981G_w. \quad \text{(water)}$$

These correlations for the water and oil configurations are illustrated in Figure 5 against the computed conductance data.

Simulations of relative permeability and saturation profiles performed using correlations and computed data in small systems show excellent agreement. Thus, the correlations are applied in simulations of saturation profiles in larger SEM images of Bentheim sandstone.

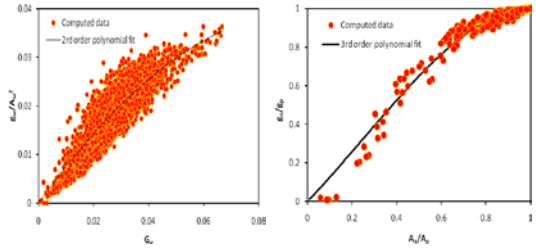

Figure 5: Conductance correlations for water and oil configurations compared with computed conductance data.

4 SIMULATION RESULTS

Simulations of saturation profile evolution are performed with the interacting tube bundle model in a Bentheim sandstone SEM image with resolution 0.204 μm and size 1134x761 pixels. Four wetting conditions are simulated; $\theta = 0^\circ, 20^\circ, 40^\circ$ and 60°.

Capillary pressure curves computed with the semi-analytical model are shown in Figure 6, and two of the corresponding cross-sectional fluid configurations are presented in Figure 7. Water layers form in pore-space constrictions, but oil invades a larger pore-space area when $\theta = 40^\circ$. Drainage displacements occur by (i) expansion of previously invaded BR regions, (ii) invasion into BR and LR region combinations that could be either connected to or disconnected from the existing oil configuration, and (iii) displacement of water layers in pore-space constrictions that are surrounded by oil. Imbibition displacements are analysed by considering the reversed order of the capillary pressures. Wettability effects on the relative permeability, computed with the conductance correlations, are found to be small.

Evolution of the saturation profiles are simulated with the interacting tube bundle model to study the effect of viscosity ratios M_v (Figure 8) and injection rates q_{tot} (Figure 9) at different wetting conditions.

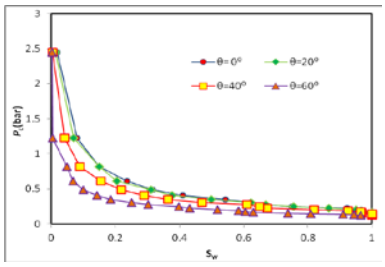

Figure 6: Capillary pressure curves computed with the semi-analytical model for different contact angles in an SEM image of Bentheim sandstone.

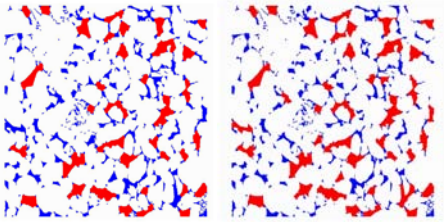

Figure 7: Oil (red) and water (blue) configurations in Bentheim sandstone computed at equal capillary pressure with $\theta = 0^\circ$ (left) and $\theta = 40^\circ$ (right).

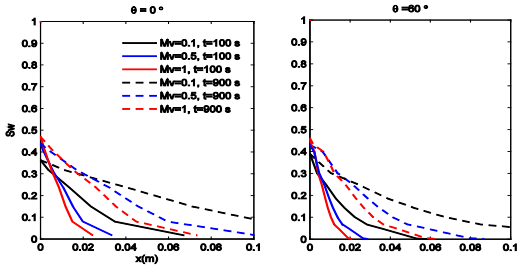

Figure 8: Effect of viscosity ratio on saturation profile evolution for free spontaneous imbibition ($q_{tot} = 0$ m^3/s) with $\theta = 0^\circ$ (left) and $\theta = 60^\circ$ (right).

The viscosity ratio has a significant impact on the saturation profiles during free spontaneous imbibition ($q_{tot} = 0$ m^3/s) for the various wetting conditions. Wettability effects for zero and moderate flow rates are presented in Figure 9. Both drainage and imbibition displacements occur at small flow rates because front menisci with large capillary pressures displace oil by water, and front menisci with small capillary pressures displace water by oil. The number of interfaces displacing oil by water increases with flow rate. The saturation fronts become steeper with increasing contact angle, but variations occur locally. For large contact angles, the most pronounced saturation changes occur in a stepwise manner, whereas more gradual fronts form for small contact angles. This is a consequence of the slightly more stepwise trends in the capillary pressure curves obtained for $\theta = 40^\circ$ and $\theta = 60^\circ$ (Figure 6), which occurs because the oil phase occupies a larger cross-sectional area of the pore space and the potential for further saturation change by movement of existing arc menisci are smaller than for $\theta = 0^\circ$ and $\theta = 20^\circ$. For high flow rates the saturation fronts become steeper with time and a Buckley-Leverett like front forms in the late stages.

5 CONCLUDING REMARKS

A model is developed for simulating viscous- and capillary-controlled displacements directly in 2D rock images. As expected, computed saturation profiles during imbibition depend strongly on viscosity ratio, injection rate and wettability. The shape of the saturation profiles computed for different wetting conditions are partly explained by the different fluid configurations occurring in the rock image.

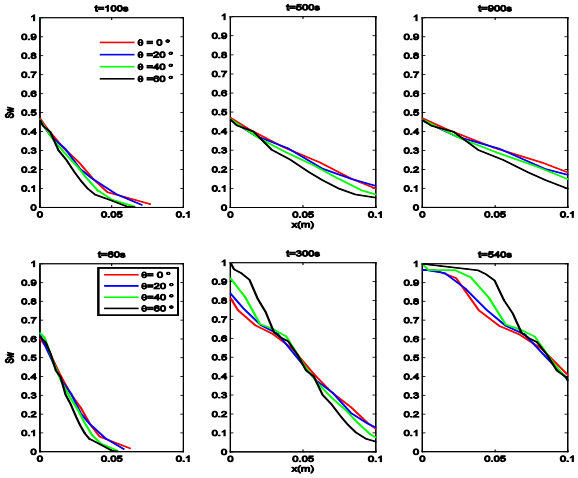

Figure 9: Evolution of saturation profiles at different wetting conditions during free spontaneous imbibition ($q_{tot} = 0$ m^3/s) (top row) and forced imbibition with flow rate $q_{tot} = 3.18\times10^{-5}$ m^3/s (bottom row).

ACKNOWLEDGMENTS

Financial support was provided by the Research Council of Norway, ConocoPhillips and the Ekofisk co-venturers, including TOTAL, ENI, Statoil and Petoro.

REFERENCES

1. Dong, M., Dullien, F. A., Dai, L., and Li, D. (2005). Immiscible displacement in the interacting capillary bundle model, Part I. Development of interacting capillary bundle model. *Transport in Porous Media*, 59, 1-18.
2. Wang, J. and Dong, M. (2011). Trapping of the non-wetting phase in an interacting triangular tube bundle model. *Chem. Eng. Sci.*, 66, 250-259.
3. Frette, O.I. and Helland, J.O. (2010). A semi-analytical model for computation of capillary entry pressures and fluid configurations in uniformly-wet pore spaces from 2D rock images. *Advances in Water Resources*, 33, 846-866.
4. Lago, M. and Araujo, M. (2001). Threshold pressure in capillaries with polygonal cross section. *J. Coll. Int. Sci*, 243: 219-226.
5. Ruth, D.W. and Bartley, J. (2002). A perfect-cross-flow model for two phase flow in porous media. International symposium of the Society of Core Analysts. Monterey, California.